TELEX The Thunderstorm Electrification and Lightning Experiment

BY DONALD R. MACGORMAN, W. DAVID RUST, TERRY J. SCHUUR, MICHAEL I. BIGGERSTAFF, JERRY M. STRAKA, CONRAD L. ZIEGLER, EDWARD R. MANSELL, ERIC C. BRUNING, KRISTIN M. KUHLMAN, NICOLE R. LUND, NICHOLAS S. BIERMANN, CLARK PAYNE, LARRY D. CAREY, PAUL R. KREHBIEL, WILLIAM RISON, KENNETH B. EACK, AND WILLIAM H. BEASLEY

Measurements during TELEX by a lightning mapping array, polarimetric and mobile Doppler radars, and balloon-borne electric-field meters and radiosondes show how lightning and other electrical properties depend on storm structure, updrafts, and precipitation formation.

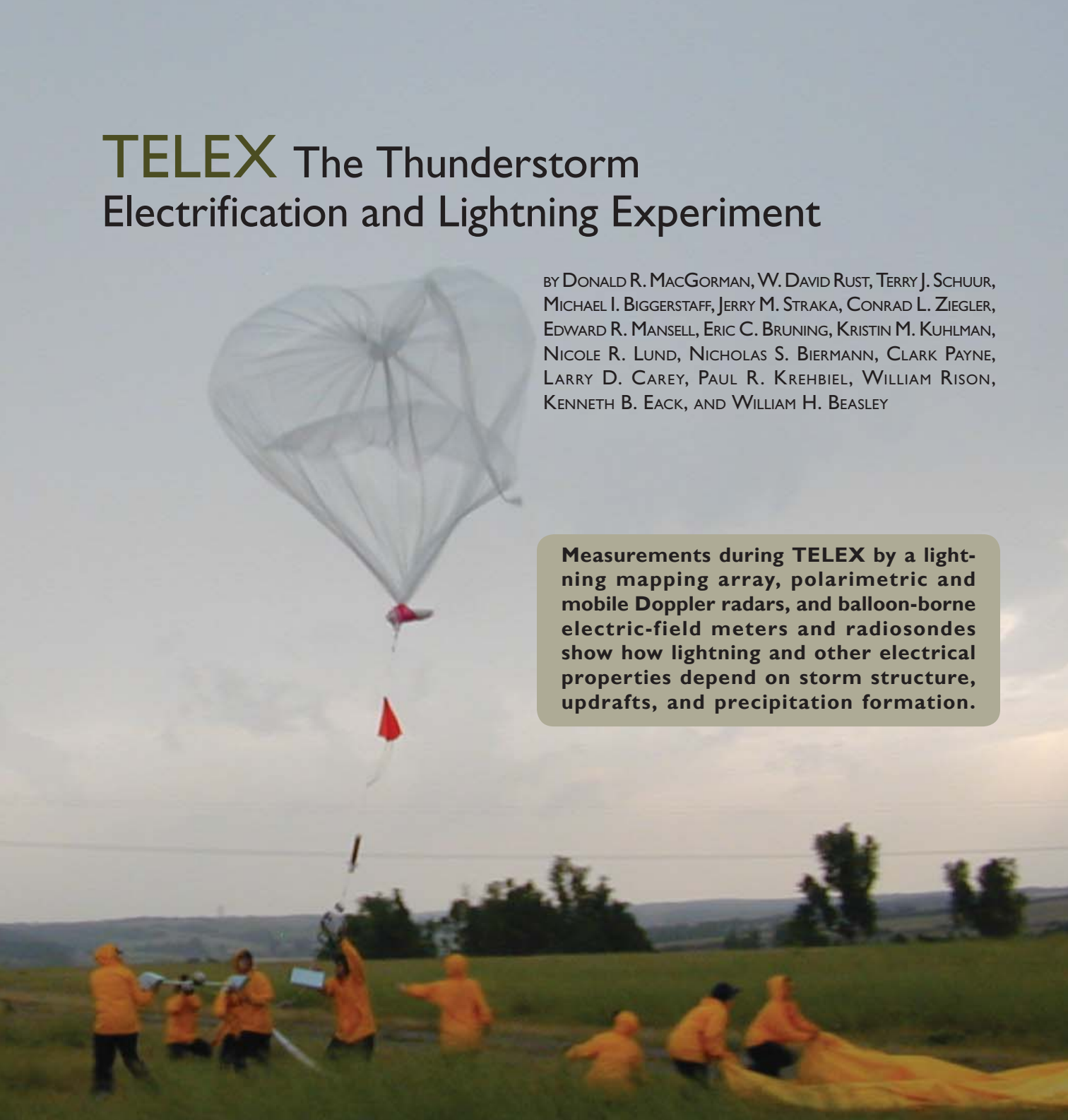

A TELEX balloon crew releases a balloon from its high-wind launch tube to fly into a supercell storm on 24 May 2004 for an in situ sounding of electric field, winds, and thermodynamic properties. Photo by Ken Eack.

In May–June 2003 and 2004, the Thunderstorm Electrification and Lightning Experiment (TELEX) brought together researchers and students from one federal and five university organizations to study how lightning and other electrical storm properties depend on storm structure, updrafts, and precipitation formation. By combining their resources, scientists employed an extensive array of sensors, including an 11-cm-wavelength polarimetric Doppler radar, two 5-cm-wavelength mobile Doppler radars, a mobile atmospheric sounding system, balloon-borne electric-field meters, an instrumented storm-penetrating T-28 aircraft, and a three-dimensional lightning mapping network. Anytime, day or night, storms occurred ▶

in central Oklahoma, teams scrambled into position to observe them. The ground-based mobile facilities acquired data for a broad spectrum of storm types on 7 days from 10 May through 5 June in 2003 and on 15 days from 15 May through 30 June in 2004.

GOALS OF TELEX. The field program had three primary emphases: 1) storms having electrical structure inverted from the usual vertical polarity, 2) lightning and other electrical properties of the stratiform region of mesoscale convective systems, and 3) developing operational applications of technologies that map all types of lightning.

Inverted-polarity electrical structure. The existence of storms having inverted-polarity electrical structure has been established only recently. In most thunderstorms, positive charge dominates in the upper region (a relatively thin region colder than roughly –25°C), and negative charge dominates the middle region (somewhere between roughly –10° and –25°C), though storms also have other charge regions, particularly at lower altitudes (e.g., Williams 1989; MacGorman and Rust 1998, 49–53; Stolzenburg et al. 1998b). Observations by the Severe Thunderstorm Electrification and Precipitation Study (STEPS) during the summer of 2000 found unexpectedly, however, that many thunderstorms on the High Plains reverse these polarities, with the upper region dominated by negative charge and the middle region dominated by positive charge (Rust and MacGorman 2002; Lang et al. 2004a; Rust et al. 2005; MacGorman et al. 2005; Wiens et al. 2005; Weiss et al. 2008). A primary goal of the STEPS field program had been to determine why the cloud-to-ground lightning activity in a large fraction of High Plains storms is dominated by flashes that lower positive charge to ground (positive ground flashes) instead of the usual negative charge (negative ground flashes). The answer appears to be that the vertical polarity of the charge structure in many High Plains storms is inverted. Now the issue is to determine why the electrical structure is inverted.

A primary goal of TELEX, therefore, was to collect additional comprehensive datasets to test and revise hypotheses that have been offered to explain how a storm's electrical structure can become inverted. All such hypotheses thus far depend on a noninductive electrification mechanism involving rebounding collisions between actively riming graupel and smaller ice particles. Over the last 10–15 yr, most of the scientific community has come to accept this mechanism as the primary one for electrifying thunderstorms, at least during initial stages (e.g., Takahashi and Miyawaki 2002; Saunders et al. 2006; discussion on pages 65–70 and 226–228 of MacGorman and Rust 1998), though other mechanisms also contribute.

This mechanism tends to put charge of one polarity on graupel and charge of the opposite polarity on smaller ice particles during rebounding collisions, followed by differential sedimentation that separates the charge by polarity into different regions as the graupel and smaller particles are transported by the wind. At moderate riming rates over most of the mixed-phase region, the noninductive mechanism tends to place negative charge on graupel and positive charge on the smaller rebounding ice particle. However, at warmer temperatures (≳–10°C) and at larger riming rates regardless of temperature in the mixed phase region, it tends to place positive charge on graupel and negative charge on the smaller ice particle. At very low riming rates, laboratory experiments have disagreed concerning the polarity and magnitude of charge that is transferred.

The usual result of these tendencies for charge distributions (though a simplified view of a typical thunderstorm) is that the negative charge that dominates at middle levels has two contributions: small ice

AFFILIATIONS: MacGorman, Rust, Ziegler, and Mansell—NOAA/OAR/National Severe Storms Laboratory, and Cooperative Institute for Mesoscale Meteorological Studies, University of Oklahoma, Norman, Oklahoma; Schuur—Cooperative Institute for Mesoscale Meteorological Studies, University of Oklahoma, and National Severe Storms Laboratory, Norman, Oklahoma; Biggerstaff, Straka, Bruning, Kuhlman, Lund, and Payne—Cooperative Institute for Mesoscale Meteorological Studies, University of Oklahoma, and National Severe Storms Laboratory, and School of Meteorology, University of Oklahoma, Norman, Oklahoma; Biermann and Beasley—School of Meteorology, University of Oklahoma, Norman, Oklahoma; Carey—Department of Atmospheric Sciences, Texas A&M University, College Station, Texas; Krehbiel, Rison, and Eack—New Mexico Institute of Mining and Technology, Socorro, New Mexico
CORRESPONDING AUTHOR: Donald R. MacGorman, National Severe Storms Laboratory/WRDD, NWC, 120 David L. Boren Blvd., Norman, OK 73072-7323
E-mail: don.macgorman@noaa.gov

The abstract for this article can be found in this issue, following the table of contents.

DOI:10.1175/2007BAMS2352.1

In final form 6 December 2007
©2008 American Meteorological Society

particles that gained negative charge at warmer temperatures and graupel that gained negative charge at somewhat colder temperatures. The positive charge in upper regions is due to small ice particles that gained positive charge at temperatures less than roughly –10°C. Storms also often have a smaller amount of positive charge in their lower regions, thought to be due at least in part to graupel that gained charge at temperatures greater than roughly –10°C (e.g., Jayaratne and Saunders 1984).

Theories to explain inverted-polarity thunderstorm charge distributions thus far have all invoked some process for increasing the riming rate of a graupel particle enough that the graupel tends to gain positive charge at all temperatures in the mixed phase region. Because inverted-polarity storms tend to occur in relatively dry environments (Knapp 1994; Carey et al. 2003) and the actual cloud liquid water content in an updraft is usually less than the adiabatic cloud liquid water profile, such suggestions have focused on mechanisms for realizing a larger fraction of the adiabatic profile in the mixed-phase region, where most charging is thought to occur. For example, MacGorman et al. (2005) pointed out that having fewer precipitation particles recycle into the updraft (due possibly to faster outflow from the upper-level updraft or drier low-level air) would reduce the number of precipitation particles accreting cloud droplets and so would reduce the loss of droplets in the updraft. Williams et al. (2005) and Carey and Buffalo (2007) suggested that the loss of cloud droplets below the mixed phase region would be reduced in storms having a higher cloud base, because of the smaller depth for depletion by warm rain processes. They also noted that updrafts having less horizontal entrainment and mixing of drier air (as in the core of broader updrafts) would realize a larger fraction of the adiabatic cloud liquid water profile.

Some data to evaluate the relative impact of these last two effects on the adiabatic profile are provided by the microphysical analyses (a combination of radar and T-28 aircraft data) of a High Plains supercell by Musil et al. (1986). Along the aircraft penetration at roughly 6–8 km MSL (approximately –9° to –30°C measured), the bounded weak echo region (BWER) and updraft exceeding 20 m s^{-1} (50 m s^{-1} maximum) both were approximately 7 km wide. Within the BWER, liquid water content increased to 3 g m^{-3} (50% of the adiabatic value) over the horizontal distance in which mixing with drier air decreased. However, in the updraft core in which constant theta-e indicated no mixing, the liquid water content eventually doubled to nearly the adiabatic value, likely because there was little precipitation accreting cloud particles there.

MacGorman et al. (2005) and Carey and Buffalo (2007) reviewed the above mechanisms, as well as others, and pointed out that different processes may be responsible for inverted-polarity electrical structure in different storms and regions. Comprehensive datasets from a variety of storm types, both normal polarity and inverted, are necessary to determine the processes that govern the vertical polarity of the charge distribution under various conditions.

Lightning in the stratiform region of MCSs. A second emphasis was to examine how the initiation and in-cloud structure of lightning in the stratiform precipitation region of different types of mesoscale convective systems (MCSs) are related to the kinematic, microphysical, and electrical structures of the systems. Most studies of MCS electrical properties thus far have examined leading-line, trailing-stratiform systems and have found that the stratiform regions of such MCSs are highly electrified. Using electric field soundings, for example, Marshall and Rust (1993) and Stolzenburg et al. (1994) showed that the charge in the stratiform region tends to occur in four to six layers, which can extend at least 100 km horizontally. Marshall and Rust estimated that a single layer can contain on the order of 10^4 C of charge, which they indicated was two to three orders of magnitude greater than most estimates for a single charge region of isolated thunderstorms (excluding the anvil) and was 2–3 times the amount estimated for a single charge layer of a severe storm anvil.

The charge layers were often less than 1 km thick, with the polarity of charge alternating from one layer to the next. At least one layer usually was warmer than 0°C. A layer at or near the 0°C isotherm usually contained positive charge. Stolzenburg et al. (1998a) developed a conceptual model of the charge distribution in leading-line, trailing-stratiform squall lines: the upper charge regions in the convective line extended far back into the stratiform region, with advection from the convective line and local generation both contributing to the charge in the stratiform region (Stolzenburg et al. 1994). Whether charge in the convective line is connected with charge in the stratiform region for any specific charge region at temperatures near or warmer than 0°C is still unknown.

Studies of lightning in leading-line, trailing-stratiform MCSs have found that the typical pattern is for frequent flashes to occur in the convective line and for sparse, infrequent, long horizontal flashes to occur in the stratiform region (e.g., Mazur and Rust

1983). Most cloud-to-ground flashes in the convective line typically are negative ground flashes, while most in the stratiform region are positive ground flashes (e.g., Rutledge and MacGorman 1988; Rutledge et al. 1990; Lang et al. 2004b). In a relatively few MCSs, positive ground flashes dominate the ground flash activity of the convective line (MacGorman and Morgenstern 1998).

Because the first of the new generation of three-dimensional lightning mapping systems was installed less than a decade ago, few studies of three-dimensional lightning mapping data for mesoscale convective systems have been published thus far. Lang et al. (2004b), Carey et al. (2005), and Dotzek et al. (2005) all examined leading-line, trailing-stratiform squall lines and found that most lightning in the stratiform region began in the upper part of the deep convective line and propagated backward and downward into a positive charge layer near the 0°C isotherm in the stratiform region. Some of these flashes did not strike ground, but some lowered positive charge to ground, sometimes doing so multiple times ≳10 km apart in a single flash. No studies published thus far have examined how lightning structure in stratiform regions is affected by the different kinematic structures of highly asymmetric MCSs, leading-stratiform, trailing-line MCSs, or chaotic MCSs (defined by Houze et al. 1990), nor have any systematically analyzed which of the multiple layers of charge in stratiform regions can be involved in lightning.

Operational applications of lightning mapping systems. A third emphasis was to develop and test applications for weather operations of systems that map all types of lightning. Cloud-to-ground lightning data have been used by the National Weather Service (NWS) for over a decade and have been useful for several applications, including detecting thunderstorm initiation and existence in various circumstances, providing rapid updates for storm motion and evolution, and detecting the large-scale configuration and reinvigoration of convection (e.g., Mosher and Lewis 1990). However, flash rates of negative cloud-to-ground lightning have essentially no relationship with severe weather (Reap and MacGorman 1989). Flash rates that include all types of lightning appear to be much more closely related to thunderstorm severity.

Both observational (e.g., Lhermitte and Krehbiel 1979; Wiens et al. 2005; Petersen et al. 2005) and modeling studies (e.g., Kuhlman et al. 2006) over the last 30 yr have demonstrated that total lightning flash rates are correlated with the volume of updraft ≥10 m s^{-1} above the 0°C isotherm, with updraft mass flux through the mixed-phase layer (for updraft ≥10 m s^{-1}), with graupel mass and volume, with column-integrated precipitation ice mass, and to a lesser extent, with cloud ice mass. Petersen et al. (2005) found that the relationship with precipitation ice mass was invariant in a bulk statistical sense across widely different climatological regimes, but most other relationships have been examined only on a storm-by-storm basis for relatively few cases. Details of most of these relationships remain to be worked out, particularly when comparing different climatological regions and types of storms. Any information about updraft trends that could be inferred from lightning data would be especially useful, as accurate trends in updraft evolution are difficult to obtain from radar in real time, yet updraft characteristics have a major influence on a storm's potential for severe weather.

Systems capable of limited detection efficiency for in-cloud flashes, in addition to high-detection efficiency for cloud-to-ground flashes, have recently become available for weather operations nationwide, and VHF mapping systems that provide much more complete lightning data have become available to the National Weather Service in various forecast offices in Alabama, Florida, Oklahoma, Texas, and the Washington, D.C., area. Also, limited products have been developed for trial use of VHF mapping data through the Advanced Weather Interactive Processing Systems in select NWS forecast offices and have been found useful, as described for example by Goodman et al. (2005). Additional developmental work is needed for operations to take advantage of the information these VHF mapping data provide to supplement radar data for warning of severe weather.

Near-term development will be focused also on applications of the total lightning data that will be provided by the lightning mapper planned for the Geostationary Operational Environmental Satellite series R (GOES-R) satellite. [Christian et al. (1989) describes the preliminary mapper design.] Spatial resolution will be reduced from the 50 m–1 km provided by VHF systems to roughly 10 km. However, coverage by the GOES-R lightning mapper is planned for the whole contiguous United States and much of the American hemisphere, and so will provide reliable thunderstorm detection and trending in large continental and oceanic regions outside the coverage of operational radars. Furthermore, lightning detection systems provide the only currently feasible technology for mapping thunderstorms globally. Several studies (e.g., Chang et al. 2001; Mansell et al.

2007) have shown that such data can be assimilated into numerical forecast models, much as radar reflectivity data are assimilated, to improve initial conditions at the start of the forecast period. However, comprehensive datasets are needed to develop these applications further.

INSTRUMENTATION. The TELEX field program took advantage of two permanently installed systems in central Oklahoma: the 11-cm wavelength KOUN polarimetric radar and the Oklahoma Lightning Mapping Array (OK-LMA). Figure 1 shows the location of each system.

The KOUN radar (Figs. 1 and 2) was originally the prototype Weather Surveillance Radar-1988 Doppler (WSR-88D) (Crum and Alberty 1993; Klazura and Imy 1993) installed in Norman, Oklahoma, but has been upgraded by the National Severe Storms Laboratory (NSSL) to add polarimetric measurements (Doviak et al. 2000; Ryzhkov et al. 2005). During TELEX, the radar collected volume scans of conventional and polarimetric data (horizontal reflectivity factor Z_h, differential reflectivity Z_{DR}, correlation coefficient ρ_{hv}, and differential phase shift Φ_{DP}) every 5–6 min. Besides providing data for analysis, KOUN also was used by nowcasters to direct and coordinate mobile facilities during TELEX operations. To help nowcasters provide guidance, the location of mobile facilities was sent to KOUN in real time via a mobile phone and plotted on a display of the radar data.

The OK-LMA (Figs. 1 and 3) maps total lightning activity, including the lightning inside clouds, in three spatial dimensions as a function of time. It was purchased from New Mexico Institute of Mining and Technology (NMIMT) by the University of Oklahoma and is operated collaboratively by the University of Oklahoma, the NSSL, and NMIMT. The OK-LMA detects a lightning flash by receiving radiation produced in a locally unused television channel (VHF channel 3) by a lightning channel segment as the channel develops. Rison et al. (1999) and Thomas et al. (2004) describe the operation and accuracy of the mapping system in detail. Complementing the OK-LMA was the commercial National Lightning Detection Network (NLDN; Cummins et al. 1998), which detected cloud-to-ground lightning strikes.

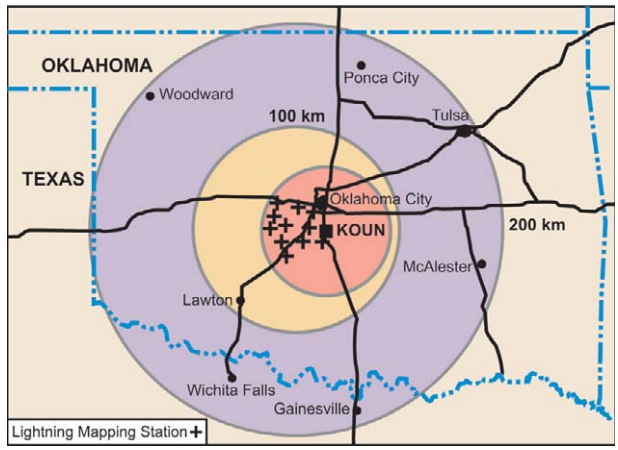

Fig. 1. Map of coverage by the Oklahoma Lightning Mapping Array and the KOUN polarimetric radar used in TELEX. Black lines depict highways. Gold shading having a radius of 100 km indicates the region in which lightning can be mapped well in three dimensions; purple shading, the 200-km nominal range within which lightning's plan location can be mapped; red shading, the region within 60 km of the KOUN radar. The majority of TELEX operations occurred within the red shading, all but two were within the gold shading, and all were within the purple shading.

The OK-LMA can map anywhere from a few to a few thousand VHF radiation sources for each flash as a function of time, to reveal the development and spatial extent of the flash. Grouping individual VHF sources into flashes is usually straightforward when the interval between flashes in a storm is ≳1 s, but becomes more difficult for shorter intervals. When the interval between flashes approaches ≲0.3 s,

Fig. 2. The KOUN polarimetric radar at the National Severe Storms Laboratory in Norman, OK, and the two mobile SMART-R C-band Doppler radars. Shown with the radars are several of the investigators from the SMART-R consortium: (from left to right) Jerry Guynes, Mike Biggerstaff, Conrad Ziegler, Lou Wicker, and Gordon Carrie.

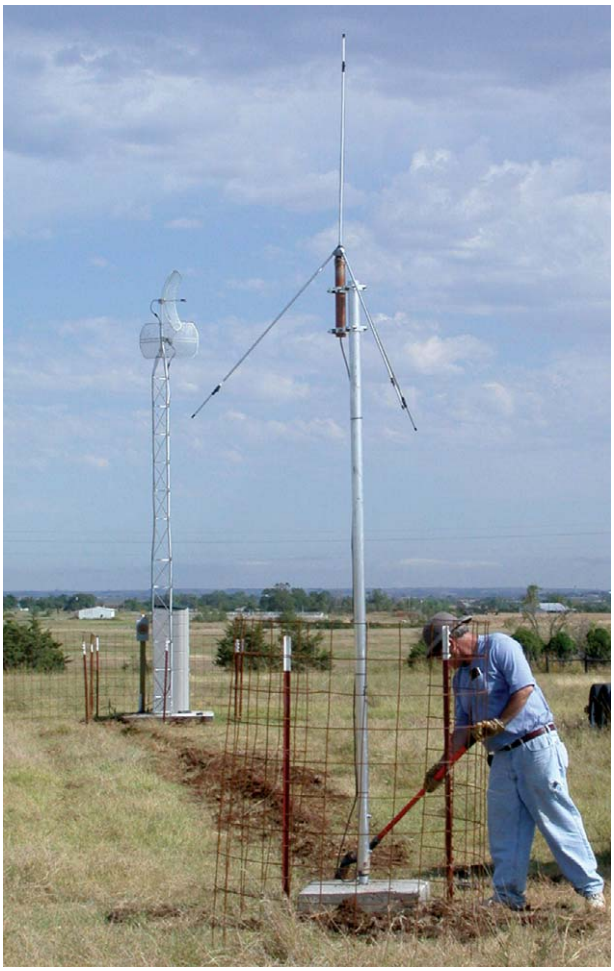

Fig. 3. A station in the OK-LMA. Lightning radiation signals are sensed by the vertical dipole antenna (foreground, near the first author of this paper). The shed that houses the station's electronics is in the background, next to antennas for communicating data to a central processing location.

flashes can be close enough in space and time that any automatic algorithm will sometimes choose incorrectly when deciding whether two or more groups of sources should be separate flashes or parts of the same flash. Occasionally the correct choice is ambiguous even when analyzing flashes manually.

All existing algorithms for automatically grouping VHF source points into flashes use the time and distance between the points as criteria. For storms within the range of three-dimensional lightning mapping, our present algorithm considers adding a new VHF source point to a flash if it occurs within 150 ms of the last point already in the flash. The new point then is actually added to the flash if it is within 500 ms and 3 km of any point already in the flash. Two segments previously treated as separate flashes are merged into one flash if the newest point added to one of the segments satisfies the 500 ms and 3-km criterion for both segments. The maximum duration permitted a flash is 3 s.

Any of these thresholds can be changed, but we have compared the results of the algorithm using these values with manual analyses of many flashes (including many in all the storms discussed later) and have found good agreement. However, when flash rates are very large, estimates by the algorithm can be sensitive to relatively modest changes in these thresholds, so estimates of large flash rates should be considered only approximate.

One can use the mapped lightning to estimate the location of the positive and negative charge regions directly involved in a lightning flash. Several studies (e.g., Kasemir 1960; Mazur 1989; Roussel-Dupre et al. 1992) have shown that lightning begins in a region of large electric-field magnitude (which tends to lie between positive and negative charge) and then propagates bidirectionally, one end propagating into and within the positive charge, and the other, into and within the negative charge (MacGorman et al. 1981; Williams 1985; Shao and Krehbiel 1996; Coleman et al. 2003). Channel development on the end propagating in positive charge produces stronger VHF signals than produced by the end propagating in negative charge (e.g., Shao and Krehbiel 1996). Because the difference is large, the first mapped VHF sources in a flash are almost always from channels moving into positive charge regions, and the OK-LMA detects many more VHF sources in positive charge regions than in negative regions (e.g., Rison et al. 1999). From the sequence of mapped flash development and the relative density of mapped sources in a region, therefore, one can often infer the location of the positive and negative charge through which a lightning flash propagated.

During TELEX in both 2003 and 2004, a mobile ballooning system (Fig. 4) was added to the KOUN radar and the OK-LMA to provide in situ soundings of storms' electrical and thermodynamic properties. NSSL's mobile laboratory carried the receivers and recorders for the balloon data. A rented truck carried enough helium, balloons, and instruments to launch six balloons into a single storm, though the data receivers allowed only four to be flying at the same time. A dropsonde system developed by the National Center for Atmospheric Research (NCAR) was modified for upsonde operation in TELEX by adding a simple baffle to redirect airflow past the temperature and relative humidity sensors. The dropsonde measured pressure, temperature, and relative humidity and provided position and winds calculated from the global positioning system (GPS; Hock and Franklin 1999).

Vector electric-field measurements were provided by a balloon-borne electric-field meter (EFM) flown with NCAR's sonde. MacGorman and Rust (1998, section 6.2.3v) discuss the design and history of this instrument, initially developed by Winn and Byerley (1975). For TELEX, the construction of the EFM was made sturdier, and onboard data recording was added to supplement telemetered data. The EFM spins about its vertical and horizontal axes at nominal rates of 1 and 3 Hz, respectively, thereby producing a sinusoidal raw signal whose amplitude is proportional to the electric-field magnitude. A two-axis accelerometer and three-axis magnetic field sensor were newly incorporated for the TELEX field program to provide improved reference signals from which the vector direction of the electric field could be determined.

Fig. 4. (top) The NSSL mobile laboratory during TELEX. (bottom left) A nighttime balloon launch. The yellow plastic sheet on the ground is the opened launch tube that had held the balloon and was opened to begin the launch. (bottom right) A balloon in flight. The instrument train for this flight consisted (top to bottom) of a parachute, an NCAR dropsonde used as an upsonde, a GPS beacon to radio the instrument's location for two days, and an electric-field meter. The lower half of the 10-m-long balloon is folded into a small square to make launching easier, but is released by a timer and unfolds soon after launch.

To make inferences about the charge distribution from measured electric fields one must rely on Gauss's law, which states that the charge density at a point is equal to a constant times the divergence in the electric field. Because we generally cannot measure all terms of the divergence from a single balloon sounding, we can face ambiguities when inferring charge density. For regions in which the horizontal derivatives are approximately zero, however (as would be expected from past measurements in much of the stratiform precipitation region of MCSs), the charge density is proportional only to the change in the vertical component of the electric field with height, which can be estimated readily from the electric-field profile measured by balloons (e.g., Stolzenburg and Marshall 1994).

In addition to the mobile facility for in situ storm measurements, another mobile facility was added in 2004 to make balloon soundings of wind and standard thermodynamic variables in the near-storm environment. Such soundings are critical to modeling studies, which use them to provide the initial conditions and possibly the time-varying lateral boundary conditions of the model domain. A commercial radiosonde, a Vaisala model RS92-SGP with GPS tracking, was flown to provide these data (Währn et al. 2004).

Also in 2004, two mobile C-band Doppler radars (Fig. 2) were added to the TELEX instrumentation suite to provide a capability for dual-Doppler synthesis of a storm's wind field and better temporal resolution than was available from the KOUN radar. These were the Shared Mobile Atmospheric Research and Teaching Radars (SMART-Rs), built and operated by a consortium of the University of Oklahoma, Texas A&M University, Texas Tech University, and the National Severe Storms Laboratory (Biggerstaff

et al. 2005). The distance between radars was typically 30–40 km. Sector volume scans, coordinated between the two SMART-R radars, typically required 2–3 min. to cover the full depth of the storm.

The South Dakota School of Mines and Technology (SDSMT) armored T-28 participated in 2003 under the direction of John Helsdon and Andy Detwiler to measure the electric field, particle charge, winds, NO_x concentration, and microphysical properties at the lower-to-middle altitudes of storms. The T-28 measured the size spectrum of water and ice particles in clouds, from cloud droplets a few micrometers in diameter to 5-cm hail. Furthermore, six electric-field meters were flush mounted around the aircraft in a configuration sufficient to measure the vector electric field. Because its operation was constrained to daylight hours, the T-28 participated in only one mission of the mobile ballooning team in 2003, but flew five other missions without mobile ballooning.

Two other groups flew additional balloon-borne instruments on a few flights. A group from NMIMT and the University of Oklahoma headed by Ken Eack and Bill Beasley flew sensors to measure X-rays and electric-field changes within the storm from lightning, to test hypotheses concerning the physics of lightning channel development. A group from the University of Washington headed by Bob Holzworth flew a prototype for measuring the electric field above storms.

OBSERVATIONS. A wide variety of storm types was sampled during TELEX. Tables 1 and 2 list the type of storm observed during each data collection operation, along with the times at which data were collected. To give an idea of the nature of the data collected, we present examples from three storms: 1) a long-lived, tornadic heavy-precipitation supercell on 29–30 May 2004, 2) a short squall line on 19 June 2004, and 3) a short-lived, small thunderstorm on 28–29 June 2004. (Plots of the lightning mapping data for these storms can be seen at http://lightning.nmt.edu/oklma.)

Tornadic heavy-precipitation supercell storm of 29–30 May 2004. On 29 May, a series of storms formed along a dryline near the border between Oklahoma and the Texas Panhandle. These storms initially moved northeast into greater boundary layer moisture. The Storm Prediction Center's outlook at 2000 UTC noted that CAPE in western Oklahoma was 4000 J kg^{-1}. Convective instability and verti-

Table 1. Summary of the 2003 TELEX operations. KOUN polarimetric radar data and OK-LMA data were collected throughout all listed times. The only operation outside the 3D coverage of the OK-LMA is indicated by 2D OK-LMA under "other measurements." The E under "other measurements" stands for electric field.

Date	EFM launch (UTC)	T-28 (UTC)	Other measurements	Storm type
14 May	0747 0818			Line of storms
16 May	0728 0744	1757–1920		Southern line of asymmetric MCS
19–20 May		2340–0108		Line of storms
20 May	0555			Small storm
23 May		1534–1643		Dissipating storm
25 May	0429		X-rays + lightning E 2D OK-LMA	Decaying supercell anvil
1 Jun		2001–2106		Storm complex
2 Jun	0425 0505 0530		X-rays + lightning E	Small squall line
4 Jun	1615 1629 1649	1606–1720	X-rays + lightning E	Asymmetric MCS
6 Jun	0311 0352			Severe MCS
10 Jun		2237–2324		Squall line

Table 2. Summary of 2004 TELEX operations. KOUN polarimetric radar data and OK-LMA data were collected throughout all listed times. The only operation outside the 3D coverage of the OK-LMA is indicated by 2D OK-LMA under "other measurements." The E under "other measurements" stands for electric field.

Date	SMART-R1 (UTC)	SMART-R2 (UTC)	EFM launch (UTC)	Environmental sounding (UTC)	Other measurements	Storm type
13 May	0209–0315	0225–0309	0205			Decaying storm
13 May			1843 1853 1903			Small storm
24–25 May	2352–0528	2343–0528	2329 2345 0007 0401	2352 0323 0418	High-altitude E	Tornadic supercell
26–27 May	2257–0230	0144–0326	2234 2242 2250 2346	2201 2332 0124		Nontornadic supercell
29–30 May	2246–0301	2207–0212	2335 2346 0012 (no EFM)	1803 2008 2237 0008 0131		Tornadic heavy precipitation supercell
2–3 Jun	2129–0416	2131–0417	0150 0231 0240	1942 2109 2231	X-rays + lightning E High-altitude E	Squall line
4 Jun	1440–1828	1412–1829		1244		Weak storms
6 Jun	0442–0540	0435–0537	0419	0341		MCS
17 Jun	1714–1222	0711–0929	0653	0800	X-rays + lightning E 2D OK-LMA	Bow echo MCS
18 Jun	0541–0649		0601 0623 0643	0442 0635		MCS
19 Jun	1252–1605	1244–1623	1242 1252 1325 1344 1455	1322	X-rays + lightning E	Small MCS
20 Jun	1545–1715	1524–1715	1537 1545 1613 1635	1507 1633		Weak storms
22 Jun	0417–0855	0410–0854	0546 0626 0702 0720			Large MCS
28–29 Jun	2340–0140	2332–0140	0020			Weak storms
30 Jun	0158–0328	0212–0332				MCS

cal shear in the horizontal winds were favorable in Oklahoma for supercell occurrence.

The southernmost storm formed at approximately 2200 UTC [1700 central daylight time (CDT)] near the southwest corner of Oklahoma and moved northeast. Around 2245 UTC, this storm began to grow rapidly. By 2330 UTC, it had taken on heavy-precipitation supercell characteristics (Doswell and Burgess 1993) and produced intermittent F0 tornadoes and hail 12 cm (4.75 in.) in diameter (Fig. 5) as storm motion turned to the right, toward the east. Mobile soundings show that the right-moving storm experienced progressively cooler, moister inflow having greater storm-relative helicity that favored increasing updraft rotation, though in a more stable environment. The storm continued intensifying through 0015 UTC, as indicated by increases both in the density and height of VHF sources (Fig. 5) and in the area and maximum reflectivity of the storm in base-scan radar data. Two sequential rain-wrapped F2 tornadoes were tracked without a noticeable break from 0017 to 0111 UTC west of Oklahoma City, Oklahoma.

Shortly after 0200 UTC, storm motion turned slightly left, toward the east-northeast. Large hail reports continued until 0410 UTC, and tornadoes continued sporadically until approximately 0700 UTC. At 0530 UTC, the horizontal area of the storm observed in base-scan reflectivity began decreasing. The storm finally dissipated at approximately 0800 UTC near the border with Arkansas and Missouri.

We analyzed data in more detail from 2330 to 0100 UTC, a period leading up to and including the first two F2 tornadoes, when the storm was well within the area of TELEX operations. The lightning activity was extreme. Estimated flash rates peaked at roughly 8 s^{-1} shortly before and during the two tornadoes and exceeded 3 s^{-1} for the entire period. (Though automatically determined flash rates this large are only approximate, as discussed previously, the above rates included only flashes composed of at least 10 mapped VHF sources, and we confirmed similar flash rates manually in spot checks. During this period, many of the flashes in the deep convec-

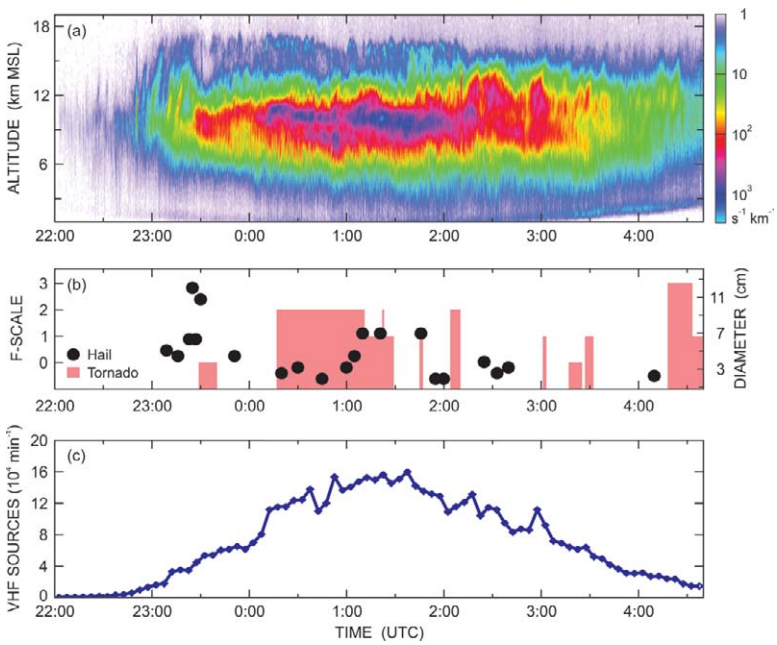

Fig. 5. Lightning, hail, and tornadoes produced by the 29–30 May 2004 heavy-precipitation supercell storm. (a) The density of sources of VHF radiation mapped by the OK-LMA as a function of height and time; colors indicate the density (number per second per kilometer of height). (b) The reported time and F-scale damage rating of tornadoes and the reported time and diameter of large hail from *Storm Data* (2004). The plotted F-scale rating of each tornado is the maximum achieved during its lifetime; at times having simultaneous tornadoes, the tornado with the largest F-scale rating is plotted. The last hail report is shown, but sporadic F0–F1 tornadoes continued longer, until 0700 UTC. (c) 5-min average of the number of VHF sources mapped per minute in this storm by the OK-LMA. In (a), note the rapid overall increase in VHF source density and the upward convective surges in the lightning data beginning shortly before 2300 UTC, a result of the development of stronger, deeper updrafts. Large hail was reported during and just after these strong surges, and the first F0 tornado began at approximately 2330 UTC, shortly after the height of lightning subsided. At this time, however, and again at approximately 0010 UTC, the VHF source density increased rapidly at 9–11 and 16–17 km MSL, the increases reflecting intensification of the storm leading to the first F0 and the first long-track F-2 tornado, respectively. These layers of larger VHF density persisted until approximately 0200 UTC, a period during which several tornadoes were produced. The larger VHF source densities changed character after 0200 UTC, as the storm track turned slightly left. After roughly 0300 UTC, the apparent decrease in lightning activity reflects primarily the decreasing detection efficiency of the OK-LMA with increasing range of the storm, and the rising minimum height of mapped VHF sources reflects the increasing height of the OK-LMA's horizon with range.

tive core of the storm were only 3–10 km in spatial extent, surprisingly small for a storm of this size.) Lightning activity extended eastward far into the downshear anvil, up to 150 km from the western edge of the storm, and some flashes were initiated in the anvil. The vertical polarity of intracloud flashes in the main body of the storm was usually inverted. Between 0000 and 0015 UTC, just before the first F2 tornado began, the intensification of the storm was reflected in the rapidly increasing VHF source densities at 9–10 and 16–17 km MSL (Fig. 5a), probably due to an increasingly strong updraft. As the tornado began, the secondary maximum in VHF source density near the top of the storm extended to the top of the 12-dB*Z* echo in the overshooting top (at an altitude of approximately 18 km MSL).

During its supercell phase, this storm produced a series of bounded minima in the horizontal projection of lightning density (often called lightning holes), each one lasting roughly 15–20 min. Lightning holes were first noted by Krehbiel et al. (2000). In a classic supercell storm in Kansas during the STEPS field program, MacGorman et al. (2005) and Wiens et al. (2005) observed that the hole tended to be located just above the BWER in the strong updraft core and probably existed for much the same reason as the BWER existed: the short residence time through the mixed-phase region in a very fast updraft would cause a relative lack there of precipitation growth and of microphysical charging from rebounding collisions between riming graupel and cloud ice. It also would allow less time for the differential sedimentation needed to separate charge macroscopically within the updraft at this level. To illustrate the relationship of the lightning holes to the reflectivity and wind structure of the 29 May storm, Fig. 6 shows lightning density and SMART-R radar data near the time the first F2 tornado touched down. The minimum lightning density in the lightning hole was aligned horizontally with the BWER and was within a core of updrafts greater than 20 m s^{-1}.

Small short-lived squall line of 19 June 2004. The mesoscale convective system for which TELEX acquired data on 19 June began as a cluster of isolated cells in southwest Oklahoma during the early morning. CAPE in central Oklahoma was modest, approximately 200 J kg^{-1}. Furthermore, there was too little vertical shear in the horizontal wind at lower levels (roughly 1 m s^{-1} km^{-1} over the lowest 6 km of altitude) to help organize the storm system. Thus, the resulting storm system was not particularly vigorous. As the cells moved northeast into south-central Oklahoma, they merged to form a leading-line, trailing-stratiform squall line (Biggerstaff and Houze 1993), with a couple of older dissipating storms embedded in the stratiform region.

At approximately 1200 UTC (0700 CDT), cells that later formed the convective line were at their tallest

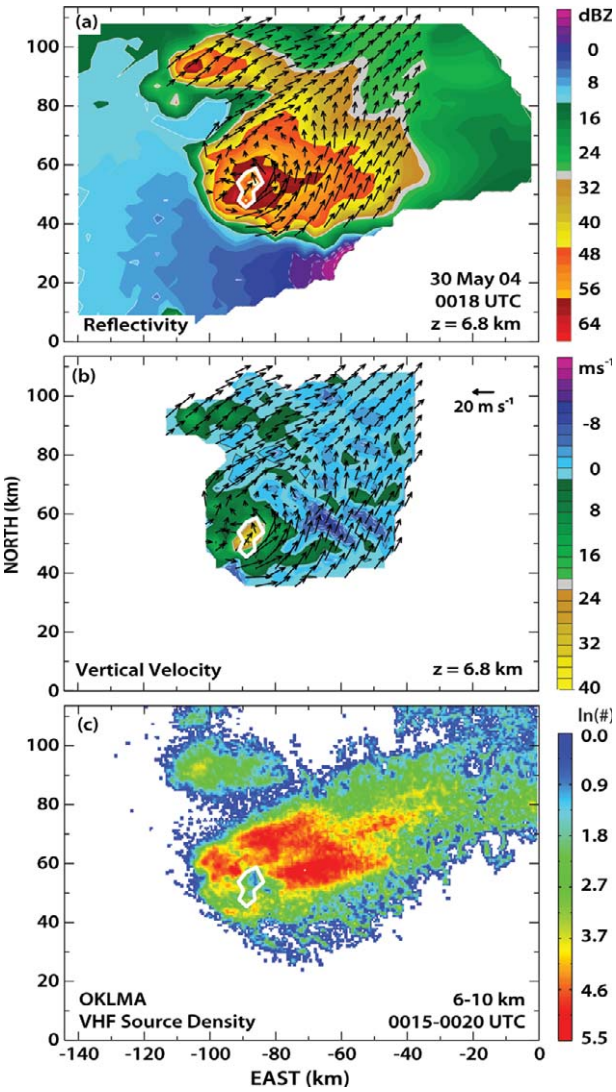

Fig. 6. (a) Radar reflectivity (color shading) and horizontal Doppler wind vectors at 6.8 km MSL, estimated from the dual SMART-R volume scans beginning at 0018 UTC 30 May 2004. (b) Vertical and horizontal wind (color shading and vectors, respectively) at the same time and altitude as in (a). The vector scale for 20 m s^{-1} applies also to (a). (c) Density of mapped VHF sources produced at 6 km $\lesssim z \lesssim$ 10 km from 0015 to 0020 UTC. The density color scale is a $\log_e$ scale. The white outline in all panels delineates the BWER. Note that the minimum lightning density in the hole is within the BWER and the core of maximum updraft speed. Coordinates are relative to the location of the KOUN radar.

(lightning extended up to 15 km MSL in several cells), though the stratiform precipitation region had not yet fully formed. At 1230 UTC, the convective line and stratiform precipitation region were fully formed. By 1300 UTC, near the beginning of data acquisition by the mobile facilities, cell heights in the convective line had decreased somewhat (lightning extended to 14–15 km MSL in the southernmost cell, but only to 12–13 km MSL in the other cells). Over the next hour, the maximum height of the convective line decreased (in all but the southernmost cell, lightning extended only to 11–12 km MSL at 1400 UTC), and the maximum reflectivity at upper levels also tended to decrease, though the system retained its leading-line, trailing-stratiform structure. As the cold pool from the system spread northeastward, thunderstorms

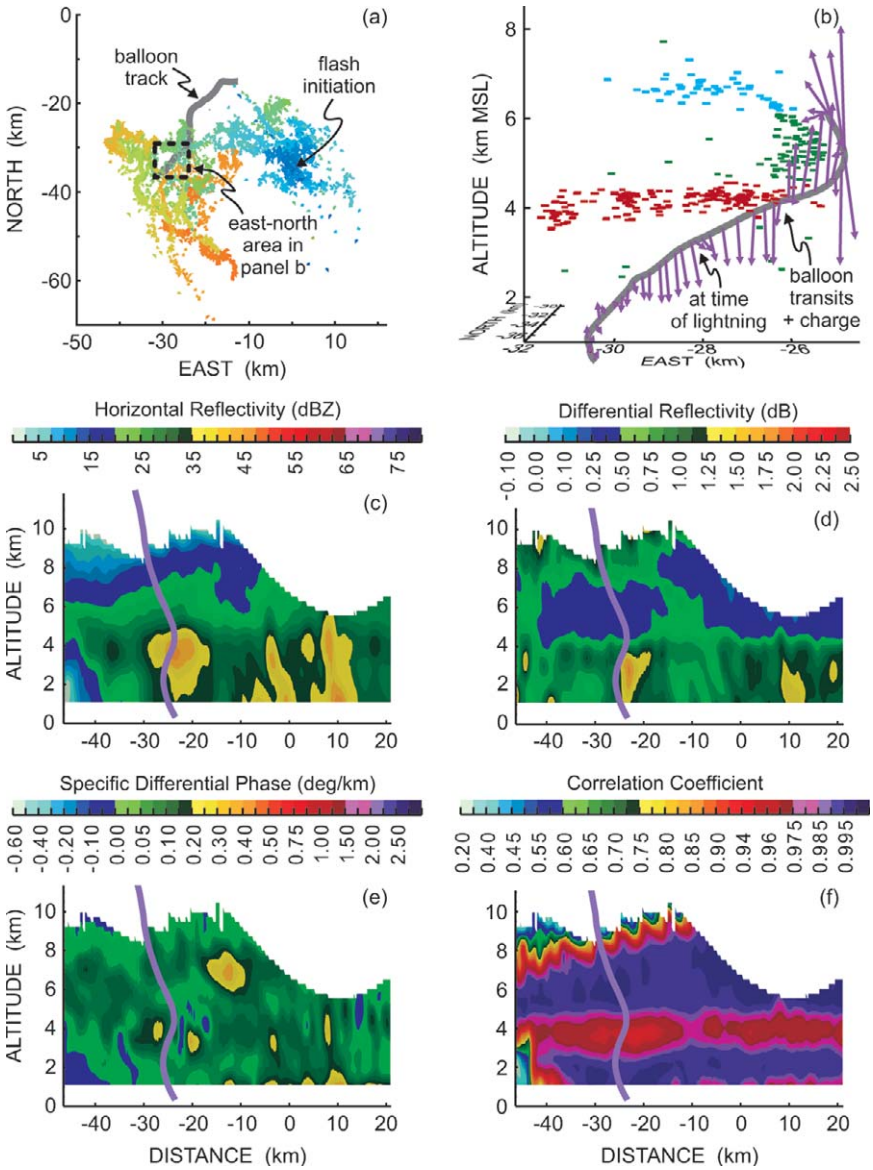

Fig. 7. (a), (b) Path of a balloon launched into the stratiform precipitation region of a squall line at 1345 UTC 19 Jun 2004, superimposed on OK-LMA data for a single flash at 1353:20.2–23.0 UTC. (a) Plan view of the whole flash. The sequence of colors indicates elapsed time, from blue through green and yellow to orange. The flash began in the convective line and propagated into the stratiform region directly above the balloon. (b) Electric-field vectors and mapped VHF sources in a three-dimensional view of the region within the dashed box in (a). The sounding is not shown above 6.7 km MSL because that is where it exited the area within the dashed box in (a). The tail of each vector is at the point on the balloon track (thick gray line) at which it was measured; only selected vectors are shown to avoid extensive overlap and make the pattern of vectors clearly visible. Red VHF sources were inferred (as described in the instrumentation section) to be from negative leaders propagating through positive charge near 4 km MSL. Blue VHF sources were inferred to be from channels propagating through negative charge near 7 km MSL. Green VHF sources were on other channels, mostly either on the lower part of the branch descending to this level from the convective line or on a vertical channel connecting the two layers of sources. Both the OK-LMA data and the electric-field data for the stratiform region indicate a layer of positive charge near 4 km MSL and a layer of negative charge just below 7 km MSL. (c)–(f) Vertical cross section of polarimetric radar parameters from the volume scan just after the lightning flash shown in (a). The storm-relative balloon track is superimposed (light-purple line). The cross section is through the balloon path and perpendicular to a weak part of the convective line (located at distance = 10 km). Each of the parameters has a relative minimum or maximum near 4 km MSL in the stratiform region. Together these indicate that the positive charge inferred from lightning and electric-field data was in the upper part of the region of aggregation and melting that forms the bright band.

continued to develop ahead of the line. Toward the end of data acquisition, as the whole system propagated northeast, these leading storms merged to form a new, longer-lasting squall line east of the region being observed, while the debris from the previous squall line was absorbed in the stratiform region.

Figure 7 gives an example of the way lightning was related to the charge distribution and the precipitation structure of the system. The balloon was launched at 1345 UTC near a relative maximum of rainfall in the stratiform region behind the convective line. Analysis of the electric-field sounding, as described in the instrumentation section, indicates that the stratiform region had ≤0.3 nC m^{-3} of negative charge density in a layer roughly 2 km thick below 3.9 km MSL and 0.5 nC m^{-3} of positive charge density in a layer 1.4 km thick just above 7.0 km MSL. Between 4 and 7 km MSL, there were four layers of charge, each 150–500 m thick (4 nC m^{-3} centered at 4.0 km MSL, –6 nC m^{-3} at 4.6 km MSL, 9 nC m^{-3} at 5.4 km MSL, and –4 nC m^{-3} at 6.7 km MSL).

The lightning flash shown in Fig. 7 occurred 3–4 min. before the balloon traversed the lowest positive charge. Our analysis (as described in the instrumentation section) of the polarity of the lightning structure shown in Fig. 7b indicates that the layer of lightning at approximately 4 km MSL was propagating through positive charge and the layer at just under 7 km MSL was propagating through negative charge, in agreement with the charge distribution inferred from the electric-field sounding. It was impossible to discern whether any channels propagated through the negative charge at 4.6 km MSL; VHF sources are sparse in negative charge regions, and the positive-charge layer at 4 km MSL through which the lightning propagated was too close to discern whether there also was a layer of sparse VHF sources at 4.6 km MSL. The flash did have a few channels propagating through the positive charge at 5.4 km MSL a short distance east of the boxed area, but had none at that level within or west of the boxed area. Most channels of the flash that could be discerned in the stratiform region were in either the positive layer centered on 4 km MSL or the negative layer just below 7 km MSL.

This flash began in the convective line and initially propagated up into positive charge at 8 km MSL. One branch propagated in positive charge at this level back toward the stratiform region and then descended gradually until it reached 4 km MSL at the southeast corner of the boxed area in Fig. 7a, near a relative maximum of precipitation from the remnants of a dissipating storm in the stratiform region. [The descent of branches in positive charge from the upper part of the convective line to approximately the 0°C isotherm in the stratiform region has been observed previously by Lang et al. (2004b), Carey et al. (2005), and Dotzek et al. (2005).] From there, this branch propagated several tens of kilometers horizontally at approximately 4 km MSL, while other channels propagated through negative charge just below 7 km MSL. Propagation through a higher layer of negative charge in the stratiform region has not been reported previously. These two layers were connected by a vertical channel in the southeast corner of the boxed region, near the location at which the descending branch from the convective line finally reached 4 km MSL. As found in the previous studies just mentioned, Figs. 7c–f show that the propagation at 4 km MSL was in the upper part of the radar bright band, identifiable from the aggregation and melting of precipitation inferred from the polarimetric data, as described by Zrnić et al. (1993).

Small storm of 28–29 June 2004. Beginning at roughly 2100 UTC 28 June, a sequence of short multicellular lines of storms formed west of the KOUN polarimetric radar. As each east–west line decayed, outflow from the decaying storms triggered the formation of a new east–west line farther north. The complete evolution of these lines was observed by the polarimetric radar and lightning mapping array. SMART-R radar data and an EFM sounding were obtained only for the last line in the sequence.

The individual cells in this last line were relatively weak. Reflectivities ≥30 dB*Z* extended above the freezing level in only a few of the cells, and only these cells produced lightning, though flash rates were relatively low. The first six lightning flashes in this line occurred from 0001 to 0008 UTC. All six struck ground and lowered negative charge from the cloud. OK-LMA data indicate that the locations at which these flashes began were clustered between 5 and 6 km MSL (–1° to –6.5°C) and within 1–2 km of one another in the horizontal. Channels for each flash propagated into a sloping layer of positive charge mostly below that level and into a layer of negative charge mostly above that level. These two charge regions did not necessarily represent the complete electrical structure of the storm at that time, as the OK-LMA reveals only those charge regions that participate in lightning.

The cluster of initiation points was located on what had been the northwest edge of an enhanced Z_{DR} column and ρ_{hv} minimum in the 2351 UTC volume scan, consistent with there having been a column containing a mixture of liquid and solid or freezing

precipitation. As shown in Fig. 8, the column of enhanced Z_{DR} was present only at lower altitudes by 2357 UTC, and a local minimum in Z_{DR} of 3–5-km horizontal extent developed between 5.5 and 6.5 km MSL (–4° to –9.5°C) near the lightning initiation points. (The minimum value of Z_{DR} was 0.2 dB.) Here, ρ_{hv} was greater than 0.99 above the melting level and showed no pronounced local minima.

As discussed by Bruning et al. (2007), these polarimetric radar signatures mean that, above the melting level, the previously enhanced Z_{DR} column had evolved by 2357 UTC from a region dominated by lofted, supercooled drops to a region of dry graupel, probably mixed with snow and cloud ice. This region of graupel was collocated with the positive charge near which flashes were initiated and through which lightning propagated. At lower altitudes, lightning channels propagated above and around the descending precipitation that had not frozen completely before warming to temperatures above 0°C. Lightning tends to propagate through regions containing net charge and around regions having little net charge (MacGorman et al. 1981; Williams 1985). The region that had contained freezing precipitation with wet surfaces would be expected to have gained little charge from interactions during rebounding graupel–ice collisions, because cloud ice particles rarely rebound from a wet surface (Saunders and Brooks 1992). Bruning et al. (2007) present a more detailed analysis of this storm, including its later stages.

SUMMARY. The TELEX field experiment provides several of the comprehensive datasets needed to investigate the relationships of lightning and storm electrification to the microphysics, winds, thermodynamics, and structure of storms. Data analysis of TELEX cases is well underway, and numerical cloud modeling studies have begun to provide complete datasets for testing hypotheses, subject to verification by observations. Of course, much more can be done with these versatile datasets. Of particular interest are the electrical behaviors of storms whose electrical structure had inverted vertical polarity, storms that produced tornadoes or large hail, and mesoscale convective systems that had highly electrified stratiform precipitation regions.

Present studies of the TELEX data add to the rapidly mounting evidence that the interaction between cloud ice and riming graupel is an essential ingredient in electrifying storms, though it may not account for every region of storm charge. The majority of flashes examined thus far began near regions of graupel, and

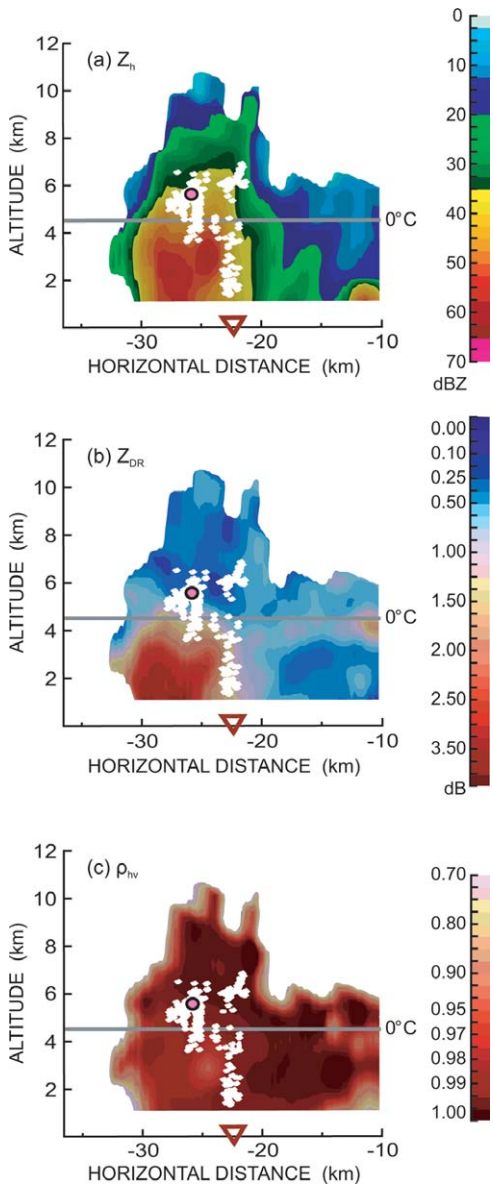

Fig. 8. The first lightning flash (0001 UTC) in a small storm on 28–29 Jun 2004 relative to polarimetric radar parameters [(a) reflectivity; (b) differential reflectivity; (c) correlation coefficient] from the volume scan beginning at 2357 UTC. White dots are the mapped VHF sources produced by this negative cloud-to-ground flash. The magenta circle marks where the flash began, and the triangle marks where it struck ground. Note that the flash was initiated near a minimum in differential reflectivity consistent with graupel, which is expected to carry charge. Its lower channels propagated around a minimum in ρ_{hv} and a maximum in Z_h and Z_{DR} consistent with rain and partially frozen hydrometeors. In previous volume scans, the precipitation now in this region had included many partially frozen particles with a wet surface, so one would expect it to have little or no charge produced by the mechanism that requires rebounding collisions between riming graupel and cloud ice. The lack of charge is consistent with lightning channels propagating around, rather than through, the region.

some channels propagated through these regions, consistent with graupel being a major charge carrier. The results of laboratory studies of charge exchange during rebounding collisions of cloud ice and actively riming graupel account for this observation qualitatively. However, the charge in some regions of storms, such as the bright band of the stratiform region of mesoscale convective systems, may involve other charging mechanisms that are poorly understood (e.g., Shepherd et al. 1996), and laboratory studies show that the magnitude and polarity of graupel and cloud ice charging are sensitive to a number of storm properties, such as the rate of graupel riming and the rate of deposition on cloud ice particles (e.g., Saunders et al. 2006). Thus, understanding what electrical behaviors the immensely complex and evolving system of a particular storm will produce is still a challenge and a goal of our TELEX studies.

Developing such understanding will help forecasters warn of storm hazards. Observational and modeling studies have found that large rapid increases in lightning flash rates are related to strong developing updrafts and to increases in graupel mass, both of which can affect a storm's potential for severe weather. Furthermore, lightning density plots have features analogous to reflectivity features related to severe weather, such as BWERs, low-level hooks, large overshooting turrets, cloud-top V features, and strong reflectivity cores. Three-dimensional lightning mapping systems capable of detecting these features are becoming more widespread. The satellite lightning mapper planned for GOES-R has poorer spatial resolution than ground-based VHF systems have, but will detect the evolving total flash rate of individual thunderstorms over all the contiguous United States. Satellite-based or very low frequency (VLF) lightning mappers are the only feasible technologies for accurately mapping thunderstorms over the entire globe, a capability that can be used for assimilation into forecast models (e.g., Chang et al. 2001; Mansell et al. 2007). Studies such as our TELEX studies help us learn how to extract the considerable useful information lightning mapping systems can provide about storm characteristics and weather hazards.

ACKNOWLEDGMENTS. TELEX data acquisition and analysis were supported in part by National Science Foundation Grants ATM-9912562, ATM-9912073, and ATM-0233268 and by Office of Naval Research Grant N00014-00-1-0525. Any opinions, findings, conclusions, or recommendations expressed in this paper are those of the authors and do not necessarily reflect the views of the National Science Foundation or the Office of Naval Research. Additional support was provided by the National Severe Storms Laboratory, the University of Oklahoma Regents, the Cooperative Institute for Mesoscale Meteorological Studies, NOAA's United States Weather Research Program, and Texas A&M University. The National Center for Atmospheric Research provided the GPS dropsonde system. The TELEX field program would have been impossible without the participation of too many people to list, including more than 30 students from the University of Oklahoma.

REFERENCES

Biggerstaff, M. I., and R. A. Houze, Jr., 1993: Kinematics and microphysics of the transition zone of the 10–11 June 1985 squall line. *J. Atmos. Sci.,* **50,** 3091–3110.

——, and Coauthors, 2005: The Shared Mobile Atmospheric Research and Teaching Radar. *Bull. Amer. Meteor. Soc.,* **86,** 1263–1274.

Bruning, E. C., W. D. Rust, T. J. Schuur, D. R. MacGorman, P. R. Krehbiel, and W. Rison, 2007: Electrical and polarimetric radar observations of a multicell storm in TELEX. *Mon. Wea. Rev.,* **135,** 2525–2544.

Carey, L. D., and K. M. Buffalo, 2007: Environmental control of cloud-to-ground lightning polarity in severe storms. *Mon. Wea. Rev.,* **135,** 1327–1353.

——, S. A. Rutledge, and W. A. Petersen, 2003: The relationship between severe storm reports and cloud-to-ground lightning polarity in the contiguous United States from 1989 to 1998. *Mon. Wea. Rev.,* **131,** 1211–1228.

——, M. J. Murphy, T. L. McCormick, and N. W. S. Demetriades, 2005: Lightning location relative to storm structure in a leading-line, trailing-stratiform mesoscale convective system. *J. Geophys. Res.,* **110,** D03105, doi:10.1029/2003JD004371.

Chang, D.-E., J. A. Weinman, C. A. Morales, and W. S. Olson, 2001: The effect of spaceborne microwave and ground-based contiguous lightning measurements on forecasts of the 1998 Groundhog Day storm. *Mon. Wea. Rev.,* **129,** 1809–1833.

Christian, H. J., R. J. Blakeslee, and S. J. Goodman, 1989: The detection of lightning from geostationary orbit. *J. Geophys. Res.,* **94,** 13 329–13 337.

Coleman, L. M., T. C. Marshall, M. Stolzenburg, T. Hamlin, P. R. Krehbiel, W. Rison, and R. J. Thomas, 2003: Effects of charge and electrostatic potential on lightning propagation. *J. Geophys. Res.,* **108,** 4298, doi:10.1029/2002JD002718.

Crum, T. D., and R. L. Alberty, 1993: The WSR-88D and the WSR-88D operational support facility. *Bull. Amer. Meteor. Soc.,* **74,** 1669–1687.

Cummins, K. L., M. J. Murphy, E. A. Bardo, W. L. Hiscox, R. B. Pyle, and A. E. Pifer, 1998: A combined TOA/MDF technology upgrade of the U.S. National Lightning Detection Network. *J. Geophys. Res.,* **103,** 9035–9044.

Doswell, C. A., III, and D. W. Burgess, 1993: Tornadoes and tornadic storms: A review of conceptual models. *The Tornado: Its Structure, Dynamics, Prediction, and Hazards, Geophys. Monogr.,* Vol. 79, Amer. Geophys. Union, 161–172.

Dotzek, N., R. M. Rabin, L. D. Carey, D. R. MacGorman, T. L. McCormick, N. W. Demetriades, M. J. Murphy, and R. L. Holle, 2005: Lightning activity related to satellite and radar observations of a mesoscale convective system over Texas on 7–8 April 2002. *Atmos. Res.,* **76,** 127–166.

Doviak, R. J., V. N. Bringi, A. V. Ryzhkov, A. Zahrai, and D. S. Zrnic, 2000: Considerations for polarimetric upgrades to operational WSR-88D radars. *J. Atmos. Oceanic Technol.,* **17,** 257–278.

Goodman, S. J., and Coauthors, 2005: The North Alabama Lightning Mapping Array: Recent severe storm observations and future prospects. *Atmos. Res.,* **76,** 423–437.

Hock, T. F., and J. L. Franklin, 1999: The NCAR GPS dropwindsonde. *Bull. Amer. Meteor. Soc.,* **80,** 407–420.

Houze, R. A., Jr., B. F. Smull, and P. Dodge, 1990: Mesoscale organization of springtime rainstorms in Oklahoma. *Mon. Wea. Rev.,* **118,** 613–654.

Jayaratne, E. R., and C. P. R. Saunders, 1984: The "raingush," lightning, and the lower positive charge center in thunderstorms. *J. Geophys Res.,* **89,** 11 816–11 818.

Kasemir, H. W., 1960: A contribution to the electrostatic theory of a lightning discharge. *J. Geophys. Res.,* **65,** 1873–1878.

Klazura, G. E., and D. A. Imy, 1993: A description of the initial set of analysis products available from the NEXRAD WSR-88D system. *Bull. Amer. Meteor. Soc.,* **74,** 1293–1311.

Knapp, D. I., 1994: Using cloud-to-ground lightning data to identify tornadic thunderstorm signatures and nowcast severe weather. *Natl. Wea. Dig.,* **19,** 35–42.

Krehbiel, P. R., R. J. Thomas, W. Rison, T. Hamlin, J. Harlin, and M. Davis, 2000: GPS-based mapping system reveals lightning inside storms. *Eos, Trans. Amer. Geophys. Union,* **81,** 21–25.

Kuhlman, K. M., C. L. Ziegler, E. R. Mansell, D. R. MacGorman, and J. M. Straka, 2006: Numerically simulated electrification and lightning of the 29 June 2000 STEPS supercell storm. *Mon. Wea. Rev.,* **134,** 2734–2757.

Lang, T. J., and Coauthors, 2004a: The Severe Thunderstorm Electrification and Precipitation Study. *Bull. Amer. Meteor. Soc.,* **85,** 1107–1125.

——, S. A. Rutledge, and K. C. Wiens, 2004b: Origins of positive cloud-to-ground lightning flashes in the stratiform region of a mesoscale convective system. *Geophys. Res. Lett.,* **31,** L10105, doi:10.1029/2004GL019823.

Lhermitte, R., and P. R. Krehbiel, 1979: Doppler radar and radio observations of thunderstorms. *IEEE Trans. Geosci. Electron.,* **GE-17,** 162–171.

MacGorman, D. R., and C. D. Morgenstern, 1998: Some characteristics of cloud-to-ground lightning in mesoscale convective systems. *J. Geophys. Res.,* **103,** 14 011–14 023.

——, and W. D. Rust, 1998: *The Electrical Nature of Storms.* Oxford University Press, 422 pp.

——, A. A. Few, and T. L. Teer, 1981: Layered lightning activity. *J. Geophys. Res.,* **86,** 9900–9910.

——, W. D. Rust, P. Krehbiel, W. Rison, E. Bruning, and K. Wiens, 2005: The electrical structure of two supercell storms during STEPS. *Mon. Wea. Rev.,* **133,** 2583–2607.

Mansell, E. R., C. L. Ziegler, and D. R. MacGorman, 2007: A lightning data assimilation technique for mesocale forecast models. *Mon. Wea. Rev.,* **135,** 1732–1748.

Marshall, T. C., and W. D. Rust, 1993: Two types of vertical electrical structures in stratiform precipitation regions of mesoscale convective systems. *Bull. Amer. Meteor. Soc.,* **74,** 2159–2170.

Mazur, V., 1989: A physical model of lightning initiation on aircraft in thunderstorms. *J. Geophys. Res.,* **94,** 3326–3340.

——, and W. D. Rust, 1983: Lightning propagation and flash density in squall lines as determined with radar. *J. Geophys. Res.,* **88,** 1495–1502.

Mosher, F. R., and J. S. Lewis, 1990: Use of lightning location data in severe storm forecasting. Preprints, *16th Conf. on Severe Local Storms,* Kananaskis Provincial Park, AB, Canada, Amer. Meteor. Soc., 692–697.

Musil, D. J., A. J. Heymsfield, and P. L. Smith, 1986: Microphysical characteristics of a well-developed weak echo region in a High Plains supercell thunderstorm. *J. Climate Appl. Meteor.,* **25,** 1037–1051.

NCDC, 2004: *Storm Data.* Vol. 46, No. 5, 580 pp. [Available from National Climatic Data Center, Asheville, NC 28801.]

Petersen, W. A., H. J. Christian, and S. A. Rutledge, 2005: TRMM observations of the global relationship between ice water content and lightning. *Geophys. Res. Lett.,* **32,** L14819, doi:10.1029/2005GL023236.

Reap, R. M., and D. R. MacGorman, 1989: Cloud-to-ground lightning: Climatological characteristics and relationship to model fields, radar observations, and severe local storms. *Mon. Wea. Rev.,* **117,** 518–535.

Rison, W., R. J. Thomas, P. R. Krehbiel, T. Hamlin, and J. Harlin, 1999: A GPS-based three dimensional lightning mapping system: Initial observations in New Mexico. *Geophys. Res. Lett.,* **26,** 3573–3576.

Roussel-Dupre, R. A., A. V. Gurevich, T. Tunnel, and G. M. Milikh, 1992: Kinetic theory of runaway air breakdown. *Phys. Rev. E.,* **49,** 2257–2271.

Rust, W. D., and D. R. MacGorman, 2002: Possible inverted-polarity electrical structures in thunderstorms during STEPS. *Geophys. Res. Lett.,* **29,** 1571, doi:10.1029/2001GL014303.

——, and Coauthors, 2005: Inverted-polarity electrical structures in thunderstorms in the Severe Thunderstorm Electrification and Precipitation Study (STEPS). *Atmos. Res.,* **76,** 247–271.

Rutledge, S. A., and D. R. MacGorman, 1988: Cloud-to-ground lightning activity in the 10–11 June 1985 mesoscale convective system observed during the Oklahoma–Kansas PRESTORM project. *Mon. Wea. Rev.,* **116,** 1393–1408.

——, C. Lu, and D. R. MacGorman, 1990: Positive cloud-to-ground lightning in mesoscale convective systems. *J. Atmos. Sci.,* **47,** 2085–2100.

Ryzhkov, A. V., T. J. Schuur, D. W. Burgess, P. L. Heinselman, S. E. Giangrade, and D. S. Zrnic, 2005: The Joint Polarization Experiment: Polarimetric rainfall measurements and hydrometeor classification. *Bull. Amer. Meteor. Soc.,* **86,** 809–824.

Saunders, C. P. R., and I. M. Brooks, 1992: The effects of high liquid water content on thunderstorm charging. *J. Geophys. Res.,* **97,** 14 671–14 676.

——, H. Bax-Norman, C. Emersic, E. E. Avila, and N. E. Castellano, 2006: Laboratory studies of the effect of cloud conditions on graupel/crystal charge transfer in thunderstorm electrification. *Quart. J. Roy. Meteor. Soc.,* **132,** 2653–2673.

Shao, X. M., and P. R. Krehbiel, 1996: The spatial and temporal development of intracloud lightning. *J. Geophys. Res.,* **101,** 641–668.

Shepherd, T. R., W. D. Rust, and T. C. Marshall, 1996: Electric fields and charges near 0°C in stratiform clouds. *Mon. Wea. Rev.,* **124,** 919–938.

Stolzenburg, M., and T. C. Marshall, 1994: Testing models of thunderstorm charge distributions with Couldomb's Law. *J. Geophys. Res.,* **99,** 25 921–25 932.

——, T. C. Marshall, W. D. Rust, and B. F. Smull, 1994: Horizontal distribution of electrical and meteorological conditions across the stratiform region of a mesoscale convective system. *Mon. Wea. Rev.,* **122,** 1777–1797.

——, W. D. Rust, and T. C. Marshall, 1998a: Electrical structure in thunderstorm convective regions. 1. Mesoscale convective systems. *J. Geophys. Res.,* **103,** 14 059–14 078.

——, ——, and ——, 1998b: Electrical structure in thunderstorm convective regions. 3. Synthesis. *J. Geophys. Res.,* **103,** 14 097–14 108.

Takahashi, T., and K. Miyawaki, 2002: Reexamination of riming electrification in a wind tunnel. *J. Atmos. Sci.,* **59,** 1018–1025.

Thomas, R., P. Krehbiel, W. Rison, S. Hunyady, W. Winn, T. Hamlin, and J. Harlin, 2004: Accuracy of the lightning mapping array. *J. Geophys. Res.,* **109,** D14207, doi:10.1029/2004JD004549.

Währn, J., I. Rekikoski, H. Jauhiainen, and J. Hirvensalo, 2004: New Vaisala radiosonde RS92: Testing and results from the field. Preprints, *Eighth Symp. on Integrated Observing and Assimilation Systems for Atmosphere, Oceans, and Land Surface,* Seattle, WA, Amer. Meteor. Soc. 4.13. [Available online at http://ams.confex.com/ams/pdfpapers/72134.pdf.]

Weiss, S. A., W. D. Rust, D. R. MacGorman, E. C. Bruning, and P. R. Krehbiel, 2008: Evolving complex electrical structure of the STEPS 25 June 2000 multicell storm. *Mon. Wea. Rev.,* **136,** 741–756.

Wiens, K. C., S. A. Rutledge, and S. A. Tessendorf, 2005: The 29 June 2000 supercell observed during STEPS. Part II: Lightning and charge structure. *J. Atmos. Sci.,* **62,** 4151–4177.

Williams, E. R., 1985: Electrical discharge propagation in and around space charge clouds. *J. Geophys. Res.,* **90,** 6059–6070.

——, 1989: The tripole structure of thunderstorms. *J. Geophys. Res.,* **94,** 13 151–13 167.

——, V. Mushtak, D. Rosenfeld, S. Goodman, and D. Boccippio, 2005: Thermodynamic conditions favorable to superlative thunderstorm updraft, mixed phase microphysics and lightning flash rate. *Atmos. Res.,* **76,** 288–306.

Winn, W. P., and L. G. Byerley III, 1975: Electric field growth in thunderclouds. *Quart. J. Roy. Meteor. Soc.,* **101,** 979–994.

Zrnić, D. S., N. Balakrishnan, C. L. Ziegler, V. N. Bringi, K. Aydin, and T. Matejka, 1993: Polarimetric signatures in the stratiform region of a mesoscale convective system. *J. Appl. Meteor.,* **32,** 678–693.